AMS Home   Journals Home   Journal Archive   Subscribe   For Authors   Help   Advanced Search   [Search] Go

Full Text View

Wind-Driven Fluctuating Western Boundary Currents

Stefano Pierini

Dipartimento di Fisica, Università dell'Aquila, L'Aquila, Italy

ABSTRACT

In this paper a linear theory for the barotropic large-scale current fluctuations at midlatitudes driven by fluctuating winds is presented. It is based on both numerical and analytical arguments and provides an extention of the steady Munk's theory of the wind-driven circulation to the case of a time-dependent wind forcing. The numerical resolution of a circulation model forced by an idealized oscillatory wind in a box leads to two distinct ranges for the oceanic fluctuating response. The first one is Rossby wavelike and westward intensified, with a width of the western boundary layer decreasing with increasing eddy viscosity A_H. For sufficiently high values of the latter, a second range arises in which the wavelike character disappears and the boundary layer width increases with A_H. To explain this behavior an analytical expression is proposed for the first (linear inertial–viscous) range in terms of an appropriate superposition of damped forced Rossby waves. Such expression provides also a length scale for the oscillating western boundary layer, which is inversely proportional to viscosity and proportional to the fourth power of the forcing frequency ω. The second (purely viscous) range corresponds to oscillating Munk's western boundary layer and Sverdrup flow in the oceanic interior. A nondimensional number, $\Gamma = A_H \beta^2/\omega^3$, is determined ($\beta$ is the variation of the Coriolis parameter with latitude), which controls the transition between the two ranges. In the inertial–viscous range $\Gamma < 1$, whereas in the purely viscous range $\Gamma > 1$.

The theory is validated by means of several numerical experiments for different values of A_H and ω and is then applied to an idealized North Atlantic. The inertial–viscous range is found to be effective for forcing periods longer than 20–40 days and shorter than 60–130 days depending on the lateral eddy viscosity, whereas the time-dependent Munk layer and Sverdrup balance are expected for longer periods. The relevance of the present theory in connection with fluctuations of the width of western boundary currents and with GCM results is discussed. The experimental evidence of wind-driven fluctuations in large-scale oceanic currents is analyzed in relation to these theoretical results.

Options:
- Create Reference
- Email this Article
- Add to MyArchive
- Search AMS Glossary

Search CrossRef for:
- Articles Citing This Article

Search Google Scholar for:
- Stefano Pierini

1. Introduction

The classical models of the wind-driven circulation and western boundary currents are steady. The Sverdrup balance for the oceanic interior, the Stommel (1948) and Munk (1950) theories proposed to close the circulation at the western boundary, and the early inertial theories all assume an atmospheric vorticity input provided by a mean time-independent wind field (e.g., Pedlosky 1996). The wind system, which induces the general circulation in the oceans, is, of course, far from being time-independent and the same can be said about the ocean circulation itself, which yields important variabilities ranging from a few days to years (e.g., Stommel 1965; Wunsch and Wimbush 1977; Düing et al. 1977; Lai 1984; Koblinsky et al. 1989; Brink 1989; Samelson 1990; Lee et al. 1990; Lee et al. 1996). In order to develop more realistic theories of the wind-driven ocean circulation it is therefore important to assess the role played by the time-dependent part of the winds in inducing oceanic variabilities in addition to those deriving from internal mechanisms. Several theoretical studies have been carried out to analyze the effect of fluctuating winds on the ocean circulation. A first effect is that of generating through nonlinear mechanisms a mean rectified circulation (e.g., Veronis 1966; Pedlosky 1967). Let us instead consider fluctuating currents induced by fluctuating winds.

Willebrand et al. (1980, hereafter denoted as WPP) studied numerically the oceanic response of the North Atlantic to the fluctuating component of the twice-daily NMC winds for the period 1973–76. The results confirm existing theories in a relatively realistic context and shed light on new aspects of the fluctuating part of the circulation. For example, they found that the large-scale [$>O(100$ km)] wind stress induces depth-independent motions for forcing periods in the range $T_{\text{inertial}} < T < 1$ yr, which are essentially linear and can account for fluctuations in the western boundary layer as high as 20–30 Sv ($\text{Sv} \equiv 10^6$ m^3 s^{-1}). Perhaps one of the most interesting results is that, while for periods between a week and a month planetary Rossby waves are dominant with an evident westward phase propagation and excitation of basin modes, for longer periods the westward propagation disappears and a time-dependent Sverdrup balance between the meridional currents and the wind stress curl is found. However, the question remains open on how, at what frequencies, and depending on what parameters the transition between the basin-mode response and the time-dependent Sverdrup balance–western boundary current takes place.

The aim of this paper is to develop a process study on the barotropic fluctuating linear ocean circulation driven by fluctuating winds. Analytical results are derived that are then validated with numerical simulations. A unified picture of the fluctuating response is thus provided, ranging from the high-frequency basin-mode response up to the low-frequency time-dependent Munk's western boundary layer and Sverdrup balance; furthermore, a qualitative description and quantitative explanation of the transition mentioned above in connection with WPP's results are given.

A linear numerical barotropic primitive equation model is implemented in a square box with dimensions typical of the North Atlantic and is forced by a spatially constant wind stress curl varying periodically in time (owing to the linearity of the problem this amounts to deriving the equilibrium response to the most general time-varying spatially constant wind stress curl). The model includes both lateral eddy viscosity and bottom friction; however, for realistic values of the forcing the eddy viscosity is the fundamental dissipative mechanism. In this sense the present model can be seen as an extension of Munk's theory of the ocean circulation to the case of purely fluctuating winds and, in fact, it tends to the well-known steady theory as the forcing frequency tends to zero.

In a recent study on the effect of shelf and slope regions on the Rossby normal modes of a basin, Pierini (1997) noticed that the forced response to a periodic wind stress is in the form of a westward intensified planetary modelike oscillation, whose width of the western boundary layer decreases with increasing lateral eddy viscosity coefficient A_H, unlike in Munk's steady western boundary currents in which the width increases as $A_H^{1/3}$. In section 2 this anomalous behavior is shown by means of an ad hoc numerical experiment; moreover, other simulations are shown corresponding to higher values of A_H for which the westward propagation vanishes and a Munk-like oscillating boundary layer arises. Two different regimes are thus identified that are studied separately in section 3.

In the first regime (section 3a) both inertial and viscous effects are important. An analytical expression in terms of an appropriate superposition of damped forced Rossby waves is constructed and is found to describe correctly the main features of the numerical solution, thus explaining satisfactorily the anomalous behavior quoted above. The usefulness of this expression lies also in the fact that it provides a length scale for the oscillating western boundary layer, which is basically made up of small-scale reflected Rossby waves. On the other hand, in section 3b it is shown that in the second regime the time rate of change of relative vorticity is negligible and a time-dependent Munk layer at the western boundary and Sverdrup balance in the oceanic interior are achieved. Apart from the different dependence upon A_H, another important difference between the two regimes is that while in the linear inertial–viscous one the width of the oscillating boundary layer depends

on the frequency of the forcing because the reflected waves are selectively dissipated by eddy viscosity, in the purely viscous regime this dependence disappears because the Munk layer depends only on the relative importance between A_H and the planetary β effect. In section 3c the transition between the two regimes is investigated. A nondimensional number Γ is derived that governs the transition: in the linear inertial–viscous range $\Gamma < 1$, whereas in the purely viscous range $\Gamma > 1$. The theory is validated by means of several numerical experiments in which A_H and the forcing period are given different values. Both the analytical flow fields and the theoretical boundary layer widths are found to compare well with their numerical counterparts.

In section 4 the formulas obtained for the two regimes are applied to the North Atlantic for typical values of the eddy viscosity coefficient. As a result, an interesting agreement with numerical results of WPP is noticed. Here we also give a more detailed description of the flow since we provide information about the smooth transition from a Rossby wavelike behavior to an oscillatory Sverdrup flow or the existence of oscillating frequency-independent western boundary layer widths, all features that are not easy to identify in a realistic numerical model. The relevance of the present theory in connection with fluctuations of the width of western boundary currents is discussed and the experimental evidence of wind-driven fluctuations in large-scale oceanic currents is also analysed in section 4 in relation with these results. Moreover, an explanation for discrepancies found when interpreting data on the basis of a time-dependent Sverdrup model is proposed. Finally in section 5 the main results are summarized and some future perspectives are discussed.

2. Basic numerical experiments

We already pointed out that the analysis presented in this paper can be seen as an extension of Munk's (1950) theory of western boundary currents to the case in which the wind stress varies sinusoidally in time. Under the linear assumption this is equivalent to studying, through a Fourier decomposition, the response to a wind stress varying arbitrarily in time. As far as the linear approximation is concerned, it is well known that in order to adjust the width of the Munk western boundary layer to a realistic width of, for instance, the Gulf Stream, the nonlinear terms in the equations of motion become comparable to the viscous terms so that nonlinear effects should be considered (e.g., Charney 1955). WPP noticed, however, that the response driven by large-scale fluctuating winds is to a good degree of accuracy linear, although its interaction with a nonlinear mean western boundary current is not, in principle, negligible. Nonetheless the linearization assumed in the present study is justified as an acceptable first step toward a more sophisticated time-dependent theory. The spatial structure of the wind is chosen so as to give a constant wind stress curl:

$$\tau_w(\mathbf{x}, t) = (by, 0) \sin(\omega t), \quad (1)$$

where $\mathbf{x} = (x, y)$ are the horizontal coordinates and b is an arbitrary constant. This choice has the advantage of being the simplest one that can drive the flows under consideration in all their basic details without introducing external length scales, which would affect the interpretation of the results. Another important reason for using (1) is that available analytical solutions of the quasigeostrophic equation forced by such a wind forcing will be used to derive important properties in the next section.

The numerical experiments are carried out by solving the linearized shallow-water equations for a homogeneous incompressible fluid of constant depth:

$$\mathbf{u}_t + f\mathbf{k} \times \mathbf{u} = -g\nabla\eta + \frac{(\tau_w - \tau_b)}{\rho D} + A_H\nabla^2\mathbf{u}$$

$$\eta_t + D\nabla\mathbf{u} = 0, \quad (2)$$

where $\mathbf{u}$ is the vertically averaged velocity, η the sea surface displacement, $f = f_0 + \beta y$ the Coriolis parameter, $\mathbf{k} = (0, 0, 1)$, g the acceleration of gravity, ρ the water density, D the water depth, τ_w the wind stress, $\tau_b = \rho C_{Db}|\mathbf{u}|\mathbf{u}$ the bottom stress, and A_H the lateral eddy viscosity coefficient. The use of a barotropic model in a flat bottom ocean at midlatitudes is justified by the virtually depth-independent nature of the flows induced by large-scale winds for forcing periods up to $O(1$ yr), although it should be noticed that, since the lower cutoff period for the first-mode baroclinic Rossby waves is $O(200$ days), for periods just below one year the response can include a baroclinic component. The theoretical considerations presented in this paper will be more conveniently based on the equation of conservation of potential vorticity in its nondivergent quasigeostrophic form:

$$\nabla^2\psi_t + \beta\psi_x = \frac{\mathrm{curl}_z\tau_w}{\rho D} + A_H\nabla^4\psi, \quad (3)$$

where ψ is the streamfunction, so that $\mathbf{u} = (\psi_y, -\psi_x)$. For the sake of simplicity of the discussion presented in the next sections, we write (3) symbolically as

$$I + P = W + V, \quad (3')$$

where I stands for linear "inertial" term, P for "planetary" vorticity, W for "wind" stress curl, and V for eddy "viscosity."

The character of the "equilibrium" periodic response of (2) to forcing (1) depends on the modal structure of the basin. In general, the response resembles the Rossby normal mode whose frequency lies near the forcing frequency ω (e.g., Pedlosky 1965; Pierini 1990), so like a normal mode it *"has fixed and moving nodes separating cells of motion, each cell alternately decreasing and then increasing in size as the moving nodes of the carrier wave approach and then pass a fixed node"* (Pedlosky 1987, p. 147). A completely different behavior is found when $\omega \gg \bar{\omega}$, where $\bar{\omega}$ is the highest eigenfrequency, in which case an oscillatory inertial boundary current is found (Flierl 1977; Pierini 1990), but in this paper we investigate the more interesting case $\omega \lesssim \bar{\omega}$. In general, any Fourier component of the wind stress generates a periodic response at equilibrium with the form described above, but—of course—those with frequencies near the eigenfrequencies of the system will excite the most energetic responses, provided that dissipative effects do not prevent multiple reflections at the boundaries and the establishment of basin modes. Therefore, we will focus our attention to the Rossby eigenfrequencies of the basin, although all the results of this paper apply equally well to any forcing frequency smaller than $\bar{\omega}$.

Figure 1a shows the Hovmöller diagram, along the central west–east section, of the meridional velocity relative to the initial value problem (1, 2) in a square box with vanishing initial conditions and no-slip boundary conditions with $L = 4000$ km, $D = 4000$ m, $f_0 = 10^{-4}$ rad s^{-1}, $\beta = 1.9 \times 10^{-11}$ rad/(m·s), $\partial\tau_x/\partial y = 0.5 \times 10^{-8}$ dyn cm^{-3} (parameters typical for the midlatitude Atlantic Ocean), $C_{Db} = 0.002$, $A_H = 10\ 000$ m^2 s^{-1}, $T = 2\pi/\omega = 24.79$ days [corresponding to the Rossby eigenperiod (4, 1), see formula (4) below and Table 1], $\Delta x = 100$ km, and $\Delta t = 60$ s.

Before proceeding to analyze the numerical results, a comment has to be made concerning the values of lateral friction used in this paper. Typical values for A_H that produce a Gulf Stream model with realistic widths range from 500 to 5000 m^2 s^{-1} (the latter being the value used by Munk in his pioneering paper). In the present model the spatial resolution used requires values of A_H larger than 5000 m^2 s^{-1} for computational stability to be assured, in fact values ranging from 10 000 to 500 000 m^2 s^{-1} will be considered, the larger ones in particular being totally unrealistic. However this does not limit the validity of the results derived in the next section: the laws governing the different dynamical regimes and the transition between them determined for unrealistic values of A_H can be extrapolated to realistic values (as done in §4) without any loss of generality.

Coming back to Fig. 1a, at equilibrium ($t > 60$–80 days) one can notice a westward intensification of the currents. In the inviscid limit $A_H \rightarrow 0$, such intensification disappears, the response being symmetrical apart from the westward phase propagation (Pedlosky 1965; Pierini 1990). On the other hand, for increasing values of A_H the longitudinal extension of the response measured from the western boundary decreases, as it appears clearly by comparing Fig. 1a with Fig. 1b, for which $A_H = 30\ 000$ m^2 s^{-1} (quantitatively we can refer to a width l_i of the western boundary layer defined in such a way that it includes most of the kinetic energy of the response; e.g., in Fig. 1a $l_i \approx 1000$ km while in Fig. 1b $l_i \approx 3 \div 400$ km). This behavior, anomalous if compared to the classical one of the steady Munk's theory, was noticed by Pierini (1997) and explained qualitatively by means of a balance of potential vorticity in which the linear inertial term I plays a decisive role, in contrast with the steady case.

A new behavior is shown here in Figs. 1c,d that corresponds to higher values of A_H. Apart from the different kind of response compared to Figs. 1a,b (virtually no propagation in the western side where most of the energy is concentrated), it should be noticed that now for increasing values of A_H the longitudinal extension of the response increases in a manner analogous to that of the steady Munk's case (now, in order to comply with the usual definition of the Munk's layer width we define a width l_v of the western boundary layer as measured up to the maximum absolute value of the meridional velocity; e.g., in Fig. 1c $l_v \approx 200$ km whereas in Fig. 1d $l_v \approx 300$ km). Therefore we are in the presence of two ranges of A_H in which very different behavior is expected for the periodic response at equilibrium. In the next section a theory is proposed that provides an explanation of such behavior.

3. A theory of fluctuating western boundary currents

The character of the westward intensified eqilibrium response to a fluctuating wind stress curl in a closed domain, as shown in the examples of Fig. 1 ⊙, is found to be quite general and always consists of two distinct ranges. In this section we propose a theoretical interpretation of this behavior. In section 3a we consider a linear inertial–viscous range for which the intensification increases with increasing lateral friction (e.g., Figs. 1a,b ⊙). We construct an analytical model for the forced response that compares well with numerical results. In doing this we reveal the mechanisms that lead to that particular response and obtain an expression for the length scale of the intensification. In section 3b we consider the second, purely viscous range (e.g., Fig. 1c,d ⊙), for which we realize that the balance $P = W + V$ holds. We then show numerically that a time-dependent Munk theory applies in this case. Finally in section 3c we introduce a nondimensional number that defines the separation between the two ranges; moreover, its consistency with numerical results is verified.

a. The linear inertial–viscous range

The behavior shown in Figs. 1a,b ⊙ evidences a westward propagation clearly due to the excitation of Rossby waves that, through reflections, establish solutions similar to forced, damped Rossby normal modes. The tendency to produce an east–west symmetrical flow in the limit $A_H \rightarrow 0$ was discussed by Pierini (1997). We therefore start from the inviscid limit given by the Rossby normal modes to build an analytical model for the westward intensified, viscous solution. The nondivergent Rossby eigenfrequencies ω_{mn} and normal modes of a rectangular domain can be easily obtained by the homogeneous and inviscid version of (3) by imposing the appropriate boundary conditions (Pedlosky 1987):

$$\omega_{mn} = -\frac{\beta}{2\pi\sqrt{\dfrac{m^2}{x_0^2} + \dfrac{n^2}{y_0^2}}}, \tag{4}$$

$$\psi_{mn} = d \cos\left(\frac{\beta x}{2\omega_{mn}} + \omega_{mn}t\right) \sin\left(\frac{m\pi x}{x_0}\right) \sin\left(\frac{n\pi y}{y_0}\right), \tag{5}$$

where $m, n = 1, 2, \cdots$, x_0 and y_0 ($\equiv L$ in our case) are the linear dimensions of the basin and d is an arbitrary constant. Table 1 ⊙ shows the first 10 zonal eigenperiods ($n = 1$) given by (4) for the parameter values defined in section 2 typical of the Atlantic Ocean. It is interesting to note that the normal mode streamfunction can also be written as the sum of four plane waves (Pedlosky 1987, §3.25):

$$\psi_{mn} = d \sum_{\pm} \cos(\mathbf{K}_{l\pm} \cdot \mathbf{x} - \omega_{mn}t)$$

$$+ d \sum_{\pm} \cos(\mathbf{K}_{s\pm} \cdot \mathbf{x} - \omega_{mn}t), \tag{6}$$

whose wavenumbers:

$$\mathbf{K}_{l\pm} = \left(-\frac{\beta}{2\omega} - \frac{m\pi}{x_0}, \ \pm\frac{n\pi}{y_0}\right),$$

$$\mathbf{K}_{s\pm} = \left(-\frac{\beta}{2\omega} + \frac{m\pi}{x_0}, \ \pm\frac{n\pi}{y_0}\right) \tag{7}$$

correspond to the same frequency given by the dispersion relation for Rossby waves ($\mathbf{K} = (k, l)$):

$$\omega = -\frac{\beta k}{k^2 + l^2}. \tag{8}$$

As an example, Fig. 2 ⊙ shows the x–t diagrams of the meridional velocity $\upsilon = -\psi_x$ for the normal modes $(1, 1)$ and $(4, 1)$ given by (5) or (6) with (7). The four waves can be grouped into two pairs, two *long* waves $\mathbf{K}_{l\pm}$ and two *short* waves $\mathbf{K}_{l\pm}$

$K_{s\pm}$ antisymmetric in y, each pair being the result of the reflection of the other pair at the opposite wall. All waves propagate their phase to the west and have the same energy flux module. However, the group velocities of the long waves have a westward component, whereas those of the short waves have an eastward component, in such a way that the sum of the energy flux vectors add to zero (no energy transmission inside the basin for each mode).

We have already stressed in section 2 that the periodic response to a spatially constant wind stress curl oscillating at a resonant frequency has, in the limit $A_H = 0$, the same form as the normal mode (6), therefore we exploit this property by taking such inviscid flow as the starting point for an analytical model of damped forced Rossby modes near the limit $A_H = 0$. We construct a meridional velocity from (6) by parameterizing the viscous damping of the short (long) waves, after reflection at the western (eastern) boundary, through an exponential decay:

$$v = -\psi_x$$

$$= d \exp\left(-\frac{x}{r_s}\right) \sum_{\pm} k_{s\pm} \sin(\mathbf{K}_{s\pm} \cdot \mathbf{x} - \omega_{mn}t)$$

$$+ d \exp\left(-\frac{L-x}{r_l}\right) \sum_{\pm} k_{l\pm} \sin(\mathbf{K}_{l\pm} \cdot \mathbf{x} - \omega_{mn}t).$$

$$(9)$$

In this simplified model the arbitrary amplitude d is not related to that of the forcing, but this is not a limitation in our context as we are only searching for sufficiently detailed information on the spatial and temporal structure of the forced flow. On the other hand, the linearity of the problem ensures that such structure does not depend on the amplitude. Let us now pass to determine the lengths r_s and r_l. From the viscous dissipation time:

$$t_D = \frac{1}{A_H K^2},$$

where $K = |\mathbf{K}|$, and from the group speed implied by (8):

$$|\mathbf{c}_g| = \frac{\beta}{K^2},$$

we can compute a decay length r in the direction of the energy flux:

$$r = |\mathbf{c}_g| t_D = \frac{\beta}{A_H K^4}.$$

We finally evaluate this formula for the short and long waves and project the resulting lengths onto the x direction:

$$r_s = \frac{\beta}{A_H K_s^4} \cos\vartheta_s, \qquad r_l = \frac{\beta}{A_H K_l^4} \cos\vartheta_l, \qquad (10)$$

where $\vartheta = \arctan(c_{gy}/c_{gx})$. This derivation of r_s and r_l is formally analogous to that used by Pedlosky (1987) to obtain a damping scale with the aim of deriving the width of Munk's layer, but an important difference should be noticed. In that calculation one assumes that the wind introduces into the system energy in a broad range of spatial and temporal scales, and the requirement that the scales be effectively trapped limits them to those that are critically damped, thus allowing one to pass from a typically time-dependent approach to a steady theory. Here, on the contrary, each Fourier component introduces only one frequency and few spatial scales, that is, those selected by the frequency circle [expression (7)], no critical damping occurs and the resulting forced flow has asymptotically the same monochromatic time dependence of the forcing itself.

The x–t diagrams of the meridional velocity for the mode (4, 1) given by (9)–(10) are presented in Figs. 3a,b for A_H = 10 000 and 30 000 m^2 s^{-1} respectively. The large difference between r_s and r_l (see Table 1) produces the westward intensification of the wavelike forced response after the transient because, while the long waves are weak and span all over the basin, the short ones are stronger and may manifest themselves intensified at the western side. The comparison with the corresponding numerical solutions of the shallow-water equations in Figs. 1a,b shows good agreement as far as shape and zonal extension of the flow are concerned. One can note a difference in the westernmost part of the basin where the no-slip boundary conditions imposed in the numerical model cannot be matched by this simple analytical model, which is also unable to reproduce the curvature of the isolines far from the western boundary in Figs. 1a,b.

In conclusion, expression (9) with (10) represents correctly the most salient features of the numerical solution in the linear inertial–viscous range such as the zonal extension of the response in the western side, which we can denote as l_i, and the westward phase propagation (further examples of the validity of this analytical model will be given in section 3c). In deriving (9) we also gained insight into the mechanisms that lead to the forced response to a fluctuating wind stress curl when both linear inertial and viscous effects are important. It should be stressed that when $l_i < L$, that is, in the presence of a substantial westward intensification, the solution, as shown in Fig. 1a,b, cannot be defined as a damped normal mode since no reflections of the short-scale Rossby waves at the eastern side take place. However, this does not limit the validity of expression (9) since it does not require multiple reflections but only a reflection of the two long waves at the western boundary and a reflection of the two short waves at the eastern boundary, all waves being continuously sustained by the wind.

Finally, when $l_i < L$ the first two terms in the rhs of (9) are predominant (cf. r_s and r_l in Table 1) and the intensification length scale can therefore be taken as equal to r_s:

$$l_i = \frac{\beta}{A_H K_s^4} \cos\vartheta_s. \qquad (11)$$

This expression will be used in section 3c to compute the separation between the linear inertial–viscous and the viscous range.

b. The viscous range

For larger values of lateral friction Figs. 1c,d show a response that differs notably from that of Figs. 1a,b analyzed in the preceding subsection. An oscillating boundary layer appears in which no propagation is present and whose width increases with increasing A_H. We can therefore presume that the viscous term has become so large that we are now in a range in which I is negligible in the potential vorticity equation (3′) so that the balance $P(\mathbf{x}, t) = W(t) + V(\mathbf{x}, t)$ reflects Munk's theory of steady western boundary currents, the time dependence entering only parametrically through the wind stress curl $W(t)$.

This hypothesis can be verified by means of the following simple numerical experiment. We force (2) through a wind stress with a curl constant both in space and in time. Figures 4a,b show the steady western boundary currents of the Munk type thus produced after a transient phase for A_H = 100 000 and 500 000 m^2 s^{-1} respectively (note the packet of short Rossby waves reflected at the western boundary during the transient in Fig. 4a for $t < 20$ days propagating eastward because of a positive group velocity, but with a westward phase propagation because of a negative phase velocity along x). Their widths compare very well with the corresponding oscillatory solutions of Figs. 1c,d. In this purely viscous range the dependence of the intensification length scale on the lateral friction is given by the well-known formula (Munk 1950):

$$l_v = \left(\frac{A_H}{\beta}\right)^{1/3}, \qquad (12)$$

which complements (11) for this purely viscous range. Another important consequence is that in the oceanic interior a time-dependent Sverdrup balance $P(t) = W(t)$ is achieved in this range.

c. The transition between the two ranges

Naturally it is important to assess a priori within which of the two ranges the solution is expected to fall for a given set of

parameters. We now proceed to determine a general criterion for this purpose. Consider the conceptual experiment in which A_H increases, all the other parameters remaining unchanged. From a complete absence of intensification for $A_H = 0$ one finds smaller and smaller values of the width of the western layer l according to (11), until a given transition width l_0 is reached. For larger values of A_H, l is now governed by (12), so that l_0 represents a minimum value for both (11) and (12). Therefore l_0 is reached when the nondimensional parameter

$$\gamma = \frac{l_v}{l_i} \tag{13}$$

is $O(1)$. Before substituting (11) and (12) into (13) we note that it is preferable to rewrite (11) in terms of the angular frequency of the forcing. Combining (11) with (8) one gets

$$l_i = \frac{\omega^4}{A_H \beta^3} \frac{\cos\vartheta_s}{(\cos\alpha_s)^4}, \tag{14}$$

where $\alpha = \arctan(l/k)$. If we now substitute (14) and (12) into (13), we finally obtain

$$\Gamma \approx \frac{A_H \beta^2}{\omega^3}, \tag{15}$$

where

$$\Gamma = \gamma^{3/4} = \frac{A_H \beta^2}{\omega^3}\delta_s, \qquad \delta_s = \frac{(\cos\alpha_s)^3}{(\cos\vartheta_s)^{3/4}} \cong 1$$

(for the position $\delta_s \cong 1$ see Table 1). If $\Gamma < 1$, we are in the linear inertial–viscous range, the balance $I + P = W + V$ holds and formula (11) applies. If $\Gamma > 1$, we are in the purely viscous range, the balance $P = W + V$ holds and formula (12) applies. The relation $\Gamma = 1$ allows us to determine either a transition value for A_H for a given ω or a transition value for ω for a given A_H. The transition width l_0 can then be computed by substituting these values either in (11) or in (12). In conclusion, under this assumption one has the following expressions for the width of the periodic western boundary layer for variable A_H [$\cos\vartheta_s \cong 1$ in (11), see again Table 1]:

$$\begin{cases} l = \dfrac{\omega^4}{A_H \beta^3}, & A_H < A_{H0} \\[4mm] l = \left(\dfrac{A_H}{\beta}\right)^{1/3}, & A_H \geq A_{H0}, \end{cases} \tag{16}$$

where for $\Gamma = 1$ one obtains $A_{H0} = \omega^3/\beta^2$ and $l = l_0 = \omega/\beta$. In Fig. 5 l given by (16) is shown for the first 10 zonal modes (Table 1) as a function of A_H. The choice of reporting the eigenfrequencies and not generic frequencies is arbitrary for those ω_{m1} in correspondence to which normal modes cannot be established (see the discussion of Fig. 8 in §4), whereas the other ω_{m1} actually represent special frequencies since a resonating response can be expected for them.

The four experiments of Fig. 1 are represented by white circles in Fig. 5 . We can easily recognize that the cases of Figs. 1a,b [mode (4, 1)] lie on the descending branch corresponding to the linear inertial–viscous range and those of Figs. 1c,d lie on the ascending branch corresponding to the purely viscous range. We notice qualitative agreement with our interpretation of the flow patterns and also quantitative agreement as far as the western boundary layer widths (as defined in section 2) are concerned.

A further validation of (16) is provided by Figs. 6 , 7 corresponding to modes (2, 1) (dots in Fig. 5) and (6, 1) (squares in Fig. 5) respectively. The case of Fig. 6a belongs to the linear inertial–viscous range and corresponds to a width of the western boundary layer (~ 12 000 km) well above the zonal length of the basin (4000 km). This implies that no

substantial intensification is to be expected, as can be verified by Fig. 6a ⊙, and that the normal mode can actually be established. In general, if the width of the western boundary layer is larger than the zonal length of the basin, then normal modes can exist. Figures 6b,c ⊙ also belong to the same range but with widths of ~ 4000 and ~ 1200 km, again in agreement with the figures. The last case lies in the viscous range just after the transition with a width of ~ 300 km. This can be verified in Fig. 6d ⊙ in which the width of the western boundary layer measured at the maximum absolute value of the meridional velocity corresponds accurately to the theoretical width. Also in agreement with the theory is the character of the response for which westward propagation is absent in the western boundary layer, being present only in a weak residual motion in the oceanic interior. Finally, for the flows of Fig. 7 ⊙ [mode (6, 1)] one could predict an inertial–viscous response for the first case and a purely viscous response for the remaining three cases, as shown by the squares in Fig. 5 ⊙. The analysis of the meridonal velocity of Fig. 7 ⊙ confirms once more the validity of the theory proposed in this section.
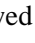
4. Discussion

In the preceding paragraph the stress was put on the dependence of the width of the fluctuating boundary layer l on the coefficient of lateral eddy viscosity. This has allowed us to validate the theory also in connection with Munk's theory of the steady wind-driven circulation. However, in order to obtain more useful information on the applicability of the theory we should adopt a different viewpoint: we assume a given value of A_H and investigate the dependence of l on the frequency of the forcing:

$$
\begin{cases}
l = \dfrac{\omega^4}{A_H \beta^3}, & \omega > \omega_0 \\[2em]
l = \left(\dfrac{A_H}{\beta}\right)^{1/3}, & \omega \le \omega_0,
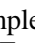\end{cases}
\tag{17}
$$

where

$$
\omega_0 = (A_H \beta^2)^{1/3} \tag{18}
$$

is the frequency at which the transition between the linear inertial–viscous and the purely viscous regimes takes place [(17) shows cearly that Munk's steady theory is the limit to which this time-dependent theory tends when $\omega \to 0$]. Figure 8 ⊙ shows $l(T)$ according to (17), where $T = 2\pi/\omega$ is the forcing period. The four thin lines correspond to the values of A_H used in the numerical experiments described in sections 2 and 3, whereas the thick solid and dashed lines correspond to the more realistic values 5000 and 500 m^2 s^{-1} respectively. The first value is the one used by Munk (1950) and WPP in their modeling studies, whereas the second is probably more realistic (Stommel 1965, chapter 8). In the following we will focus our attention on the first of these values so that we will be able to comment on our results in comparison with those of WPP.

First of all, one can notice that l equals the zonal length of the basin $L = 4000$ km for $T \equiv T_L \approx 20$ days, that is, at a forcing period larger than those of the first three basin modes (see the upper side of the graph). This implies that no substantial intensification is present for those frequencies and, therefore, multiple reflections and the resonant excitation of such normal modes are allowed (Fig. 6a ⊙ is an example of this case for a different value of viscosity). In general, one can define a timescale T_L,

$$
\omega_L = (LA_H \beta^3)^{1/4} \tag{19}
$$

so that for $T < T_L$ basin modes can exist provided that, of course, T is larger than the fundamental eigenperiod T_{11} defined by (4) [note that in this range also free modes can exist, being excited by bursts of winds, for example, as shown in the context of topographic Rossby modes by Pierini (1996)]. On the other hand, for $T_L < T < T_0$, where $T_0 \approx 60$ days is defined through (18), we are in the linear inertial–viscous range with substantial intensification, corresponding to a forced response in terms of westward intensified, westward propagating forced Rossby waves of the kind of those shown in Figs. 1a,b ⊙, just to give an example. The fluctuating boundary layer width decreases very rapidly with T until the purely viscous range is reached. Finally for $T > T_0$ the forced response is in terms of an oscillating Munk layer with a width independent of ω and an instantaneous Sverdrup balance in the oceanic interior (for $A_H = 500$ m^2 s^{-1} one would obtain $T_L \approx 40$ days and

$T_0 \approx 130$ days).

This is in good qualitative and quantitative agreement with the more realistic modeling results of WPP briefly discussed in the introduction. In their numerical study on the oceanic response of the North Atlantic represented by a rectangle to the fluctuating component of the twice-daily NMC winds for the period 1973–76, the authors found that for periods between a week and a month planetary Rossby waves are dominant, with an evident westward phase propagation and excitation of basin modes. Here we found this behavior from 8.5 to 20 days. Moreover, for periods longer than a month they noticed that the westward propagation disappears and a time-dependent Sverdrup balance between the meridional currents and the wind stress curl is achieved. In the present study we obtained an even more detailed description of this dynamics: the disappearence of the westward propagation takes place smoothly as T increases within what we called the linear inertial–viscous range, which spans between 20 and 60 days. Although the westward propagation begins to vanish before T_0, it is for $T > T_0$ that it is totally absent and the Sverdrup balance in the oceanic interior holds. WPP also noticed that for periods between the inertial period and a week the response is not wavelike but is locally forced. This can be theoretically explained, for instance, by means of the analytical treatments by Flierl (1977) and Pierini (1990). In the latter an analytical solution was proposed as being continuously valid for both the high frequency, oscillatory boundary layer, and the Rossby wavelike behavior.

Thus, apart from providing some new theoretical background for the interpretation of more realistic numerical results, two new details of information have been obtained that complement WPP's description of the wind-forced dynamics. The first is the existence of the linear inertial–viscous range that connects smoothly the basin mode circulation with the time-dependent Sverdrup balance, and the second is the Munk-like character of the time-dependent circulation near the western boundary when the Sverdrup balance holds away from it, in the purely viscous range. The existence of the linear inertial–viscous range can probably explain also a result by WPP concerning the sensitivity of the response to different values of A_H. For viscosity only three times as large (15 000 instead 5000 $m^2 \, s^{-1}$) they found that kinetic energy spectra in a midocean station show a substantial decrease of energy, particularly for frequencies corresponding to or larger than the basin modes. This could be accounted for by the westward intensification in the linear inertial–viscous range for which the energy is redistributed preferentially to the west, thus reducing the signal in the center of the basin.

Another interesting aspect implied by (16), (17) and related to the last point discussed above concerns the width of a realistic western boundary layer composed of a mean and a fluctuating part. The presence in the wind spectrum of energy in the linear inertial–viscous range induces fluctuations that widen the western region in which the currents are intensified. In other words, fluctuations in the linear inertial–viscous range increase the total width of the western boundary layer beyond that of the mean Munk layer, the width in excess being therefore given by a superposition of western intensified Rossby waves and a residual steady Sverdrup flow. Fluctuations in the viscous range, on the other hand, modulate the mean western bounday current without altering the total width. Thus, if the variability in current measurements taken near the western coast of a large ocean yields episodes of strong inertial–viscous oscillations, then a wavelike extension of the current system beyond the mean western boundary current is to be expected.

Finally, let us proceed to analyze some experimental evidence of wind-driven barotropic fluctuations in large-scale oceanic currents. The relevance of the atmospheric forcing in inducing an important part of the variability in the Gulf Stream was observed, for instance, by Wunsch and Winbush (1977) and Düing et al. (1977). Lee et al. (1990) reported current meter measurements taken along a zonal section east of the Bahamas in which a surprisingly large variability in the barotropic transport over the section was found. Meridional transport variations as large as 90 Sv in 1.5 months were found to occurr in the upper layer and simultaneously, with similar transport events, in the deep western boundary current. The barotropic nature of these strong fluctuations suggests that the wind (both as a remote and local forcing) can be considered as a possible candidate for their generation. More recently Lee et al. (1996) found in the same location evidence of a predominantly barotropic response to remote and local seasonal wind forcing. Examples of experimental investigations for which large-scale current fluctuations were attributed explicitly to the wind are those by Koblinsky et al. (1989), Brink (1989), Samelson (1990), and more recently, using TOPEX/Poseidon altimeter data, by Isoguchi et al. (1997) and Stammer (1997).

The results of the present paper may provide some new theoretical background for the interpretation of these experimental data. In particular, in some of the studies cited above a relation between wind stress curl fluctuations and either current measurements or SSH anomalies was searched for by using a time-dependent Sverdrup model for the oceanic interior. Although an interesting agreement is generally found, some important discrepancies are nonetheless evident. One of the possible reasons for their occurrence is that the Sverdrup model was used without any particular attention to the frequency range for which it should hold. For example, if in a simple flat-bottom "North Atlantic" box model (such as ours) one constructed a Sverdrup flow from monthly averages of a given time-dependent wind stress curl taken as the forcing and compared such flow with the numerical response for an ambient eddy viscosity of the order of 500 $m^2 \, s^{-1}$, then good agreement could not be found because (as seen above) for periods as high as $T < T_0 \backsimeq 130$ days forced Rossby normal

modes are expected rather than a time-dependent Sverdrup balance. On the other hand, for 5000 m^2 s^{-1} monthly averages of wind-derived Sverdup flows would compare relatively well with the response because now $T_0 \cong 60$ days, but the comparison would be even more satisfactory if the high frequency winds corresponding to the linear inertial–viscous range were filtered out or if the winds were averaged over longer intervals. This simple example suggests more realistic process studies which could help interpreting experimental data of this nature.

5. Conclusions

In this paper, a theory has been proposed, based on both numerical and analytical arguments, for the barotropic large-scale oceanic current fluctuations at midlatitudes driven by fluctuating winds in a period range from $O(10 \text{ days})$ to $O(1 \text{ yr})$ under the assumption that the problem is linear and that the horizontal eddy viscosity is the fundamental dissipating mechanism. Two regimes have been identified. There is a linear inertial–viscous range for which the response is Rossby wavelike and westward intensified, a measure of the intensification being given by the length scale

$$l_i = \frac{\omega^4}{A_H \beta^3}.$$

In this range an analytical expression for the current system is proposed that compares well with numerical results. There is, moreover, a purely viscous range for which the Rossby dynamics is suppressed and the flow field corresponds to a time-dependent Munk's theory, that is, an instantaneous Sverdrup balance in the oceanic interior and an oscillating boundary layer with width

$$l_v = \left(\frac{A_H}{\beta} \right)^{1/3}.$$

A nondimensional number has been determined,

$$\Gamma = \frac{A_H \beta^2}{\omega^3},$$

which specifies the transition between the two ranges. For $\Gamma < 1$ we are in the linear inertial–viscous range, whereas for $\Gamma > 1$ the viscous regime holds. For a given value of the eddy viscosity one can outline the following scenario for the generic forcing period:

1. $T_{\text{inertial}} < T < T_{11}$: no wavelike, locally forced response

2. $T_{11} < T < T_L$: forced Rossby normal modes

3. $T_L < T < T_0$: westward intensified forced Rossby waves

4. $T_0 < T$: oscillating Munk layer and Sverdrup balance,

where T_{11} is the fundamental Rossby eigenperiod of the basin, T_L is the period for which in the linear inertial–viscous regime the western boundary layer width equals the zonal length of the basin, and T_0 is the period corresponding to $\Gamma = 1$, that is, for which the transition between the linear inertial–viscous and the purely viscous regimes takes place [the corresponding angular frequencies $\omega_{11}, \omega_L, \omega_0$ are given by (4), (19), and (18) respectively]. The theory has been applied to the case of an idealized North Atlantic for which $T_{11} \cong 8.5$ days, $T_L \cong 20$ (40) days, and $T_0 \cong 60$ (130) days for A_H = 5000 (500) m^2 s^{-1}. Naturally we should bear in mind that these ranges were obtained in a flat-bottom box model with a simplified forcing; also the use of a constant eddy viscosity was certainly a rough schematization, though it is quite common in numerical modeling. Thus no direct extrapolation can be made to the real North Atlantic, nonetheless these idealized results have evidenced dynamical behaviors that are expected to exist—though modified in various ways—in real oceans. On the other hand, only by means of an oversimplified model such as this could one grasp novel and general mechanical features of the fluctuating wind-driven oceanic response.

These results extend Munk's theory to the case of the most general time dependence of the wind forcing in the

framework of a simplified box model. They also provide an explanation of the anomalous intensification of the periodic western boundary currents observed numerically by Pierini (1997). An interesting agreement with numerical results of the model of the North Atlantic forced by NMC winds by Willebrand et al. (1980) was noticed. In addition, the present results give also a more detailed description of the flow, such as for instance the smooth transition between a Rossby wavelike behavior and the oscillating Sverdrup flow in the interior or the existence of oscillating western boundary layers, all features that are not easy to identify in a realistic numerical model. The relevance of the present theory in connection with fluctuations of the width of western boundary currents was discussed. The experimental evidence of wind-driven fluctuations in large-scale oceanic currents was also analyzed in relation with the present theoretical results. Finally, an explanation for discrepancies found when interpreting data on the basis of a time-dependent Sverdrup model was proposed.

The study carried out in this paper, apart from being helpful in interpreting some aspects of the variability of currents in western boundary currents, can turn out to be useful also in controlling the response of general circulation models of large oceans. For example, often the value of eddy viscosity in a numerical model must be chosen larger than a realistic value simply in order to damp unresolved scales, as was the case in the numerical examples presented in this paper. In such a case it is well known that the structure of a mean western boundary current is affected by that. However, one should be aware that also the fluctuating part of the wind-driven response is dramatically sensitive to unrealistically high values of A_H, as discussed in this paper. This is because, apart from a reduced amplitude of the response, a larger value of Γ is implied with the consequence that part of the wind spectrum will now fall in the viscous range whereas it would produce inertial–viscous oscillations for a more realistic A_H, in so modifying the overall spatial structure of the barotropic wind-driven variability.

Future perspectives foresee a generalization of these results to the case in which nonlinear, baroclinic, topographic effects, more realistic winds, and the equatorial region are included. Nonlinearities, known to be important in steady theories of western boundary currents, appear to play a less important role for wind-driven fluctuating currents, although both the interaction of the latter with the mean flow induced by mean winds and the self-advection of the fluctuations deserve to be studied. Baroclinic effects are not important in a flat ocean in the temporal range considered here, but they may become locally important especially near the coasts where topographic variations are relevant. Also the presence of a midocean ridge on the character of the response should be investigated. Finally, a further extension of these results concerns their baroclinic counterpart, which interests variabilities at timescales longer than $O(200$ days$)$. The analysis of some of these aspects is under way.

REFERENCES

Brink, K. H., 1989: Evidence for wind-driven current fluctuations in the western North Atlantic. *J. Geophys. Res.,* **94,** 2029–2044..

Charney, J. C., 1955: The Gulf Stream as an inertial boundary layer. *Proc. Natl. Acad. Sci. U.S.A.,* **41,** 731–740..

Düing, W. O., C. N. K. Mooers, and T. N. Lee, 1977: Low-frequency variability in the Florida Current and relations to atmospheric forcing from 1972 to 1974. *J. Mar. Res.,* **35,** 129–161..

Flierl, G. R., 1977: Simple applications of McWilliams' "A note on a consistent quasigeostrophic model in a multiply connected domain." *Dyn. Atmos. Oceans,* **1,** 443–453..

Isoguchi, O., H. Kawamura, and T. Kono, 1997: A study on wind-driven circulation in the subarctic North Pacific using TOPEX/Poseidon altimeter data. *J. Geophys. Res.,* **102,** 12 457–12 468..

Koblinsky, C. J., P. P. Niiler, and W. J. Schmitz Jr., 1989: Observations of wind-forced deep ocean currents in the North Pacific. *J. Geophys. Res.,* **94,** 10 773–10 790..

Lai, D. Y., 1984: Mean flow and variabilities in the Deep Western Boundary Current. *J. Phys. Oceanogr.,* **14,** 1488–1498..

Lee, T. N., W. Johns, F. Schott, and R. Zantopp, 1990: Western boundary current structure and variability east of Abaco, Bahamas at 26.5°N. *J. Phys. Oceanogr.,* **20,** 446–466..

——, ——, R. J. Zantopp, and E. R. Fillenbaum, 1996: Moored observations of western boundary current variability and thermohaline circulation at 26.5°N in the subtropical North Atlantic. *J. Phys. Oceanogr.,* **26,** 962–983..

Munk, W. H., 1950: On the wind-driven ocean circulation. *J. Meteor.,* **7,** 79–93..

Pedlosky, J., 1965: A study of the time dependent ocean circulation. *J. Atmos. Sci.,* **22,** 267–272.. Find this article online

——, 1967: Fluctuating winds and the ocean circulation. *Tellus,* **19,** 250–256..

— , 1987: *Geophysical Fluid Dynamics.* Springer-Verlag, 710 pp..

— , 1996: *Ocean Circulation Theory.* Springer-Verlag, 453 pp..

Pierini, S., 1990: A divergent quasi-geostrophic model for wind-driven oceanic fluctuations in a closed basin. *Dyn. Atmos. Oceans,* **14,** 259–277; Corrigendum: **14,** 415..

— , 1996: Topographic Rossby modes in the Strait of Sicily. *J. Geophys. Res.,* **101,** 6429–6440..

— , 1997: Westward intensified and topographically modified planetary modes. *J. Phys. Oceanogr.,* **27,** 1459–1471..

Samelson, R. M., 1990: Evidence for wind-driven current fluctuations in the eastern North Atlantic. *J. Geophys. Res.,* **95,** 11 359–11 368..

Stammer, D., 1997: Steric and wind-induced changes in TOPEX/Poseidon large-scale sea surface topography observations. *J. Geophys. Res.,* **102,** 20 987–21 009..

Stommel, H., 1948: The westward intensification of wind-driven ocean currents. *Trans. Amer. Geophys. Union,* **29,** 202–206..

— , 1965: *The Gulf Stream.* University of California Press, 248 pp..

Veronis, G., 1966: Generation of mean ocean circulation by fluctuating winds. *Tellus,* **18,** 67–76..

Willebrand, J., S. G. H. Philander, and R. C. Pacanowski, 1980: The oceanic response to large-scale atmospheric disturbances. *J. Phys. Oceanogr.,* **10,** 411–429..

Wunsch, C., and M. Wimbush, 1977: Simultaneous pressure, velocity and temperature measurements in the Florida Straits. *J. Mar. Res.,* **35,** 75–104..

Tables

Table 1. First 10 zonal eigenperiods of the square domain under consideration according to [formula (4)](#) (T_{mn} are in days) with the corresponding values of $\cos\vartheta_s$, $\cos\alpha_s$, and δ_s defined in [section 3](#). The values r_s and r_l defined by [(10)](#) are in kilometers and refer to the case $A_H = 10\ 000\ \mathrm{m^2\ s^{-1}}$.

m	n	T_{mn}	$\cos\vartheta_s$	$\cos\alpha_s$	δ_s	r_s	r_l
1	1	8.50	0.71	0.92	1.023	75 725	2 572 412
2	1	13.44	0.89	0.97	1.002	12 445	4 007 143
3	1	19.01	0.95	0.99	1.001	3119	4 497 153
4	1	24.79	0.97	0.99	1.000	1080	4 700 725
5	1	30.66	0.98	1.00	1.000	462	4 801 782
6	1	36.57	0.99	1.00	1.000	228	4 858 645
7	1	42.51	0.99	1.00	1.000	125	4 893 631
8	1	48.47	0.99	1.00	1.000	74	4 916 625
9	1	54.44	0.99	1.00	1.000	46	4 932 524
10	1	60.42	1.00	1.00	1.000	31	4 943 965

Click on thumbnail for full-sized image.

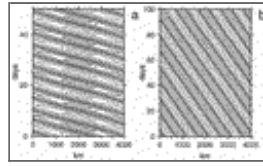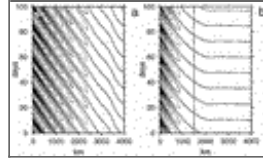## Figures
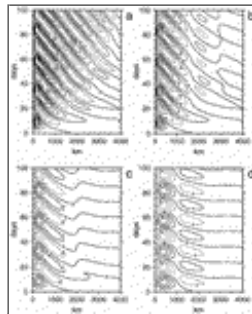
Click on thumbnail for full-sized image.

Fig. 1. Hovmöller diagrams of the meridional velocity υ (in mm s^{-1}) solution of [(2)](#) forced by [(1)](#) with $\omega = \omega_{41}$ ($T = 24.79$ days)

along a zonal section equidistant from the northern and southern boundaries with (a) $A_H = 10\ 000\ \text{m}^2\ \text{s}^{-1}$, (b) $A_H = 30\ 000\ \text{m}^2\ \text{s}^{-1}$, (c) $A_H = 100\ 000\ \text{m}^2\ \text{s}^{-1}$, (d) $A_H = 500\ 000\ \text{m}^2\ \text{s}^{-1}$.
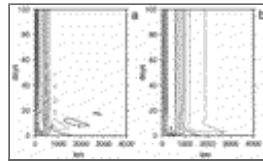

Click on thumbnail for full-sized image.

Fig. 2. Hovmöller diagrams of the meridional velocity υ given by the analytical inviscid nondivergent normal modes (1, 1) (a) and (4, 1) (b) given by (5) or (6) with (7) along a zonal section equidistant from the northern and southern boundaries.

Click on thumbnail for full-sized image.

Fig. 3. Hovmöller diagrams of the meridional velocity υ given by expression (9) with (10) and $\omega = \omega_{41}$ ($T = 24.78$ days) along a zonal section equidistant from the northern and southern boundaries with (a) $A_H = 10\ 000\ \text{m}^2\ \text{s}^{-1}$ (cf. Fig. 1a ⦿), (b) $A_H = 30\ 000\ \text{m}^2\ \text{s}^{-1}$ (cf. Fig. 1b ⦿).
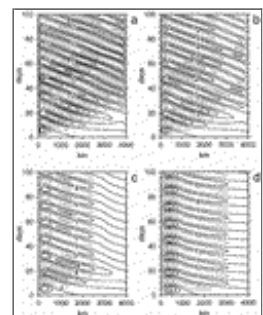

Click on thumbnail for full-sized image.

Fig. 4. Hovmöller diagrams of the meridional velocity υ (in mm s^{-1}) solution of (2) forced by a wind stress curl constant both in space and time along a zonal section equidistant from the northern and southern boundaries with (a) $A_H = 100\ 000\ \text{m}^2\ \text{s}^{-1}$ (cf. Fig. 1c ⦿), (b) $A_H = 500\ 000\ \text{m}^2\ \text{s}^{-1}$ (cf. Fig. 1d ⦿).
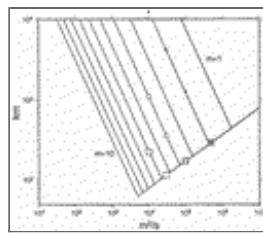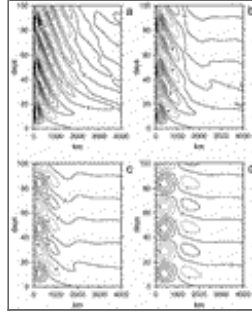

Click on thumbnail for full-sized image.

Fig. 5. Width of the fluctuating western boundary layer l vs the horizontal eddy viscosity coefficient A_H according to (16) for the first 10 zonal eigenperiods given in Table 1 ⦿. The white circles denote the experiments of Fig. 1 ⦿, the dots those of Fig. 6 ⦿, and the squares those of Fig. 7 ⦿.
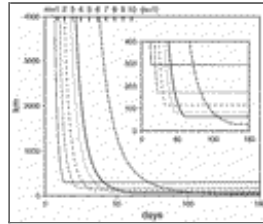

Click on thumbnail for full-sized image.

Fig. 6. Hovmöller diagrams of the meridional velocity υ (in mm s^{-1}) solution of (2) forced by (1) with $\omega = \omega_{21}$ ($T = 13.44$ days) along a zonal section equidistant from the northern and southern boundaries with (a) $A_H = 10\ 000$ m^2 s^{-1}, (b) $A_H = 30\ 000$ m^2 s^{-1} (c) $A_H = 100\ 000$ m^2 s^{-1}, (d) $A_H = 500\ 000$ m^2 s^{-1}.

Click on thumbnail for full-sized image.

Fig. 7. Hovmöller diagrams of the meridional velocity υ (in mm s^{-1}) solution of (2) forced by (1) with $\omega = \omega_{61}$ ($T = 36.57$ days) along a zonal section equidistant from the northern and southern boundaries with (a) $A_H = 10\ 000$ m^2 s^{-1}, (b) $A_H = 30\ 000$ m^2 s^{-1}, (c) $A_H = 100\ 000$ m^2 s^{-1}, (d) $A_H = 500\ 000$ m^2 s^{-1}.

Click on thumbnail for full-sized image.

Fig. 8. Width of the fluctuating western boundary layer vs the forcing period according to (17) for $A_H = 500\ 000$ m^2 s^{-1} (thin solid line), $A_H = 100\ 000$ m^2 s^{-1} (thin dashed–dotted line), $A_H = 30\ 000$ m^2 s^{-1} (thin dashed line), $A_H = 10\ 000$ m^2 s^{-1} (thin dotted line), $A_H = 5000$ m^2 s^{-1} (thick solid line), $A_H = 500$ m^2 s^{-1} (thick dashed–dotted line).

Corresponding author address: Prof. Stefano Pierini, Dipartimento di Fisica, Università dell'Aquila, Via Vetoio, I-67010 Coppito (L'Aquila), Italy.

E-mail: Stefano.Pierini@aquila.infn.it

top ▲